We are IntechOpen, the world's leading publisher of Open Access books Built by scientists, for scientists

4,800
Open access books available

122,000
International authors and editors

135M
Downloads

Our authors are among the

154
Countries delivered to

TOP 1%
most cited scientists

12.2%
Contributors from top 500 universities

WEB OF SCIENCE™

Selection of our books indexed in the Book Citation Index in Web of Science™ Core Collection (BKCI)

Interested in publishing with us?
Contact book.department@intechopen.com

Numbers displayed above are based on latest data collected.
For more information visit www.intechopen.com

Chapter 2

Cancelling Harmonic Power Line Interference in Biopotentials

Țarălungă Dragoș Daniel and
Mihaela Neagu (Ungureanu)

Additional information is available at the end of the chapter

http://dx.doi.org/10.5772/intechopen.74579

Abstract

Biopotential signals, like the electrocardiogram (ECG), electroencephalogram (EEG), electromyogram (EMG), and so on, contain vital information about the health state of human body. The morphology and time/frequency parameters of the biopotentials are of interest when diagnostic information is extracted and analyzed. The powerline interference (PLI), with the fundamental PLI component of 50 Hz/60 Hz and its harmonics, is one of the most disturbing noise sources in biopotential recordings that hampers the analysis of the electrical signals generated by the human body. The aim of this chapter is to review the existing methods to eliminate harmonics PLI from biopotential signals and to analyze the distortion introduced by some of the most basic approaches for PLI cancelation and whether this distortion affects the diagnostic performance in biopotentials investigations.

Keywords: biopotentials, power line interference, harmonics, diagnostic

1. Introduction

At the cellular level, the movement of ions like K^+, Na^+, Ca^{2+} and Cl^- determines the presence of biopotentials at the level of the cellular membrane. When a stimulus arrives on the membrane, an action potential is generated and is transmitted to the neighboring cells, spreading within the entire tissue or just within some parts of the tissue, depending on the presence of inhibitory channels. At the macroscopic level, the sums of all the action potentials generate a biopotential. By placing electrodes on the human body, in specific configurations, a projection of the investigated biopotentials on the measurement direction may be recorded. Basically,

every human body tissue has associated an electromagnetic field, which can be theoretically measured. However, usually the biopotentials have a very low power (amplitude of μV), thus just a few can be recorded: the electrical activity generated by the cardiac tissue, the electrocardiogram (ECG), by the brain, the electroencephalogram (EEG), by the skeletal muscles, the electromyogram (EMG), by the uterus, electrohysterogram (EHG), by the retina, the electroretinogram (ERG), by the stomach muscles, the electrogastrogram (EGG), by the fetal cardiac tissue, the fetal electrocardiogram (fECG), and so on. All these signals contain diagnostic information about the health status of the source tissue, which can be extracted by applying different signal processing methods.

Nevertheless, the raw signals recorded after the measurement cannot be used directly to evaluate the health status of the source tissue because it contains also noise, which in most of the cases hampers the extraction of diagnostic information. The disturbing biopotentials (e.g., when the fECG analysis is of interest, the mECG, which is also recorded, represents a noise source and has to be eliminated) or other noise sources like electronic noise (thermal noise, shot noise, flicker noise) and power line interference have to be canceled/diminished. The latter is one of the most common types of noise in biopotential recordings, and its efficient cancelation is still an open question in biomedical signal processing. Therefore, the optimal elimination of the noise sources is critical since any residual or disturbance introduced by the cancelation method can impair the diagnostic information and could lead to a wrong diagnostic.

Thus, in this chapter, a review of the principal methods for removing PLI from biopotentials is introduced. Also, a case study reveals the influence on the diagnostic parameters of the most common PLI cancelation methods applied in ECG analysis. The chapter has the following sections:

- Sources of the PLI and its harmonics—this section presents the most common sources of the PLI and the ways it usually interferes with biopotential measurements.
- Methods for canceling PLI and its harmonics—this section includes a review of the recent methods for PLI removal from biopotentials.
- The influence of bandstop filters on the diagnostic parameters of the ECG signals—this section describes the morphological parameters of the ECG signal which are used to make a diagnostic, the filters used, the data considered and the results obtained.

2. Sources of the PLI and its harmonics

The PLI is generated by the alternative 50/60 Hz sinusoidal current from the power grid. However, the PLI has also hamonics due to the fact that the PLI is in most of the cases non-sinusoidal. This is caused usually by the so-called "non-linear" loads connected to the power grid.

A load which draws a proportional current with the applied voltage is considered to be linear (e.g., loads that are purely resistive or that are simple combinations of pure resistance, inductance or capacitance). They do not change the shape of the waveform current but may change the phase between the current and the applied voltage.

http://dx.doi.org/10.5772/intechopen.74579

On the other hand, nonlinear loads draw non-sinusoidal current even when sinusoidal voltage is applied (**Figure 1**). Thus, nonlinear loads change the shape of the current waveform from a sine wave to some other form and create harmonic currents in addition to the original (fundamental frequency) AC current. In turn, these harmonic currents will cause harmonic voltages to be generated. According to the IEEE 519-2014, the harmonic is a sinusoidal component of a periodic wave or quantity having a frequency that is an integral multiple of the fundamental frequency or a component of order greater than one of the Fourier series of a periodic quantity [1].

The main nonlinear loads consist of the static power converters (rectifiers, **Figure 2**) that are used in switch-mode power supplies, uninterruptable power supplies, and so on. Thus, fluorescent lamps, medical devices, personal computers, induction motors, and so on represent nonlinear loads connected to the power grid and sources of harmonics [2, 3].

Moreover, it seems that some harmonics have a greater impact than others. For example, the third harmonic is probably the most challenging one in terms of neutral conductor loading within a three-phase system (the most common method used by electric power distribution grids worldwide to distribute power). However, other harmonics currents cancel each other out in the neutral point (like normal 50 Hz load current), third harmonics are in phase with each other, and the summing in the neutral conductor significantly increases the current [4].

There are different ways in which the PLI interferes with the biopotential recordings [5]:

- *Magnetic induction*: the cables used for biopotential recordings can form a loop, and if a variable magnetic field is present, then a potential will be induced in the leads which is proportional with the area and orientation of the loop, and the magnitude of the magnetic field.
- *Displacement current into recording leads*: by capacitive coupling between the AC power line and the leads, a current is induced in the recording leads, which is called displacement current. The latter disturbs the recording just if the impedances of the electrode-skin interfaces are different, because in this case, the "potential divider effect" appears, that is, common mode interference is converted into differential mode interference voltage which

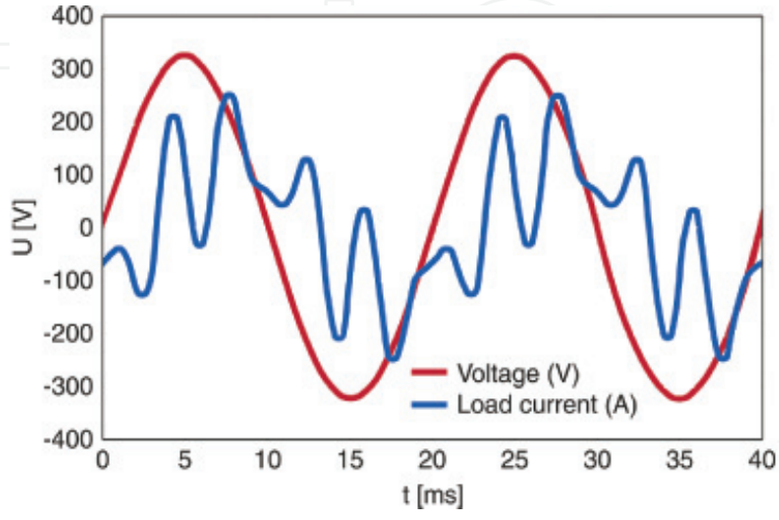

Figure 1. The sinusoidal voltage and the current generated by a nonlinear load.

is amplified. In this case, not even an instrumentation amplifier with infinitely high common mode rejection ratio (CMRR) will make any difference.

- *Displacement current into the body*: because of parasitic capacities, the body is capacitive coupled with the AC power lines. The displacement current travels through the body to the ground and because the body has impedance, a voltage drop will appear. Hence at different locations on the body, the induced potential is at slightly different values which in turn are amplified by the instrumentation amplifier.

In **Figure 3**, a schematic representation of the way the displacement currents are induced in the measurement setup is illustrated.

Empirical solutions can be applied in order to reduce the amount of PLI and its harmonics present in the biopotential measurements: twisting the recording leads will reduce the area between them, and thus the induced current from the variable magnetic field is much smaller; the preparation of the skin before attaching the electrode is going to reduce and balance the electrode-skin impedance so that the difference between the two impedances is as small as possible; movement of the ground electrode, and so on.

However, in spite of all the precautions taken before measuring, the PLI is still going to interfere with the recorded biopotentials. Nevertheless, because most of the biopotentials have low power, any PLI disturbance, even if much attenuated by different approaches, will impair the analysis of the diagnostic information.

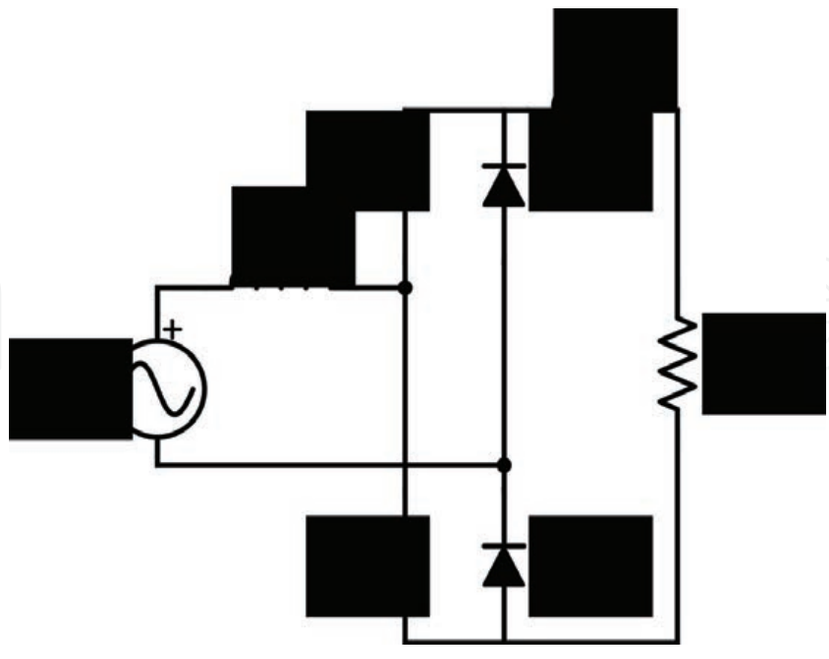

Figure 2. A load containing an inductance (L_{dc}) and a resistance (R_{dc}) is supplied from a single-phase full wave diode bridge rectifier.

http://dx.doi.org/10.5772/intechopen.74579

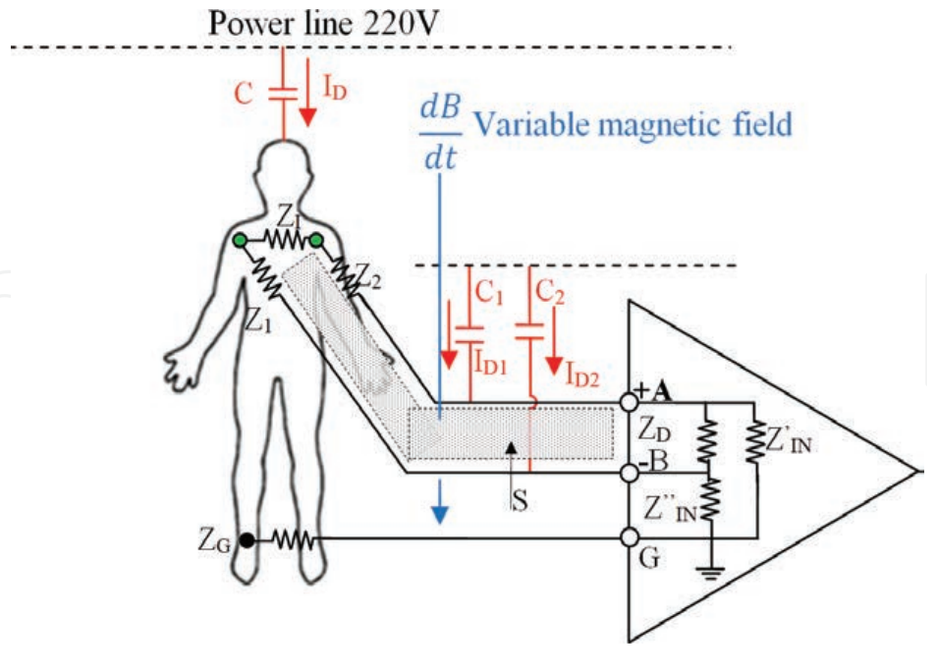

Figure 3. Capacitive coupling between the power line and the measurement leads and the human body: I_D—the displacement current in the human body; C—coupling capacity between the power line and the human body; I_{D1}, I_{D2}—the displacement current in the measurement leads; Z_I—the impedance of the human body between the two electrodes; Z_1, Z_2—the impedance of the electrodes; Z_G—the impedance of the ground electrode; Z_D—the differential input impedance of the instrumentation amplifier; Z_{IN}—the input impedance of the instrumentation amplifier; C_1, C_2—the coupling capacities between the power line and the measurement leads; S—the area described by the measurement leads.

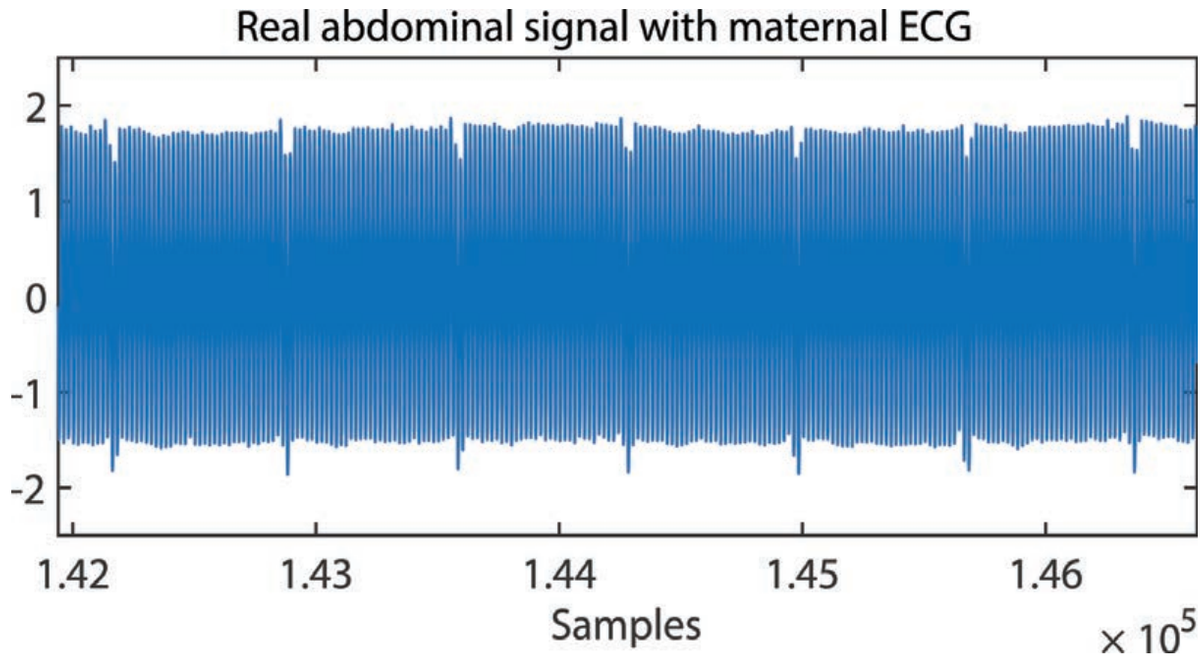

Figure 4. Abdominal recorded signal with strong PLI contamination.

In **Figure 4**, a real measurement of biopotentials recorded on the abdomen of a pregnant woman is depicted. By visual inspection, it can be observed that only the PLI and its harmonics are visible.

3. PLI and harmonic cancelation methods

The main problem when considering removing the PLI is that the frequency bandwidths of the biopotentials include the 50/60 Hz fundamental frequency and also the third harmonic (**Figure 5**). Thus, the method for PLI cancelation should ideally not remove useful information too.

There are many approaches for removing PLI and harmonics from biopotential measurements. The most common hardware solutions mainly consist of implementing hardware notch filters [6]. Another common hardware approach is the right leg driven (DLR) circuit [7], which is used to reduce the common mode interferences. A recent paper proposes a new version of the classical DLR circuit, reporting an improvement of 30 dB in reducing the PLI [8]. However, recent studies suggest that this approach can increase actually, in some situations, the interference [9].

In this chapter, we focus on software methods for PLI and harmonics removal. The main software methods for PLI cancelation are: (1) band stop digital filters; (2) fixed—frequency notch filters; (3) neural networks; (4) adaptive filters; (5) blind source separation; (6) Kalman filters; (7) time-frequency processing of nonstationary signals (wavelet transform); (8) subtraction methods; (9) spectral Hampel filter; (10) time-frequency nonlinear analysis of nonstationary signals (empirical mode decomposition—EMD, Hilbert Huang Transform—HHT) [10].

In **Table 1**, a selection of recent contributions in PLI removing from biopotentials is introduced.

Loss of information can appear when the methods for PLI cancelation are applied. Thus, methods for information retrieval are also implemented. In [11], the authors apply the EMD

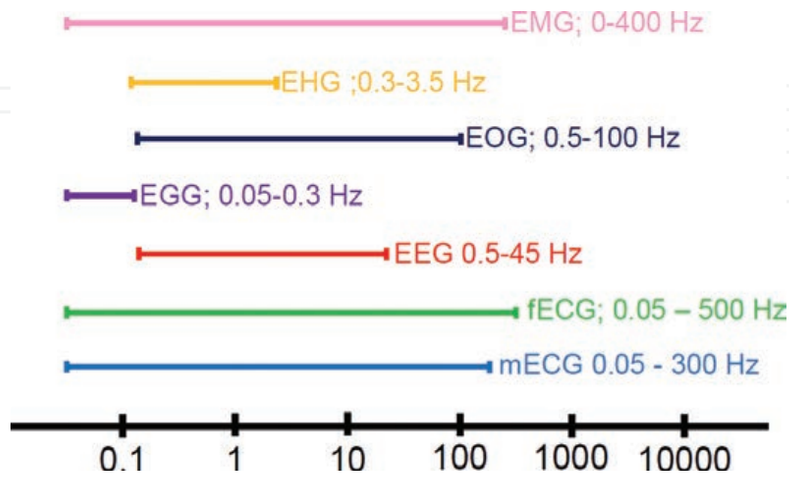

Figure 5. Frequency domain of different biopotentials.

Time-varying pole radius multiple notch filters			
Authors	**Year**	**Biopotentials**	**Observations**
Piskorowski [12]	2012	ECG	A time-varying pole radius multiple notch infinite impulse response (IIR) filter is introduced. The performance is evaluated on ECG signals and compared with traditional time-invariant notch filters. A significant reduction in transient time is reported in comparison with the traditional notch filters. The filter is evaluated also in [6] on removing the PLI from abdominal signals in order to extract the fECG showing a good performance: root mean square deviation (RMSD) of 2.11% and signal-to-noise ratio (SNR) improvement of 76 dB
Piskorowski [13]	2013	EMG	A modified version of the algorithm introduced in [14] is proposed by finding optimal nonzero initial conditions (based on vector projection algorithm) for reduction of transient time of IIR digital notch filters. The modification consists of choosing the length of the initial segment to cover the PLI fundamental frequency. The filter is applied on canceling the PLI from the EMG signals with good results
Rana et al. [15]	2017	ECG	Introduces a time varying pole-radius filter based on a hyperbolic tangent sigmoid function in order to achieve high-quality factor and short transient duration. The performance is assessed on PLI cancelation from ECG signal in the LabVIEW-based simulation reporting better results than similar approaches
a. Adaptive filters			
Wang et al. [16]	2017	–	Proposes an adaptive filter based on least mean square (LMS). In the first step, simplified all-pass filter is introduced to construct an IIR non-adaptive notch and then an adaptive LMS filter is applied. The performance is evaluated in different scenarios, also including up to three harmonics and it is compared with cascaded notch filters in multiple narrow bands interference suppression. This filter is not evaluated on biopotentials
Razzaq et al. [17]	2016	ECG	An adaptive filter for PLI and its harmonics suppression with no reference signal is proposed. It is based on recursive state space model and is evaluated on ECG signals. While good performance is reported, high computational complexity still remains an issue
Lin et al. [18]	2016	EEG	Introduces an adaptive framework for PLI removal from EEG signals when both the reference and the signal are contaminated with spike noise. M-estimation function is used for robustness of the adaptive filter to the influence of impulse components. Based on this approach, LMS and normalized LMS (NLMS) are extended to least mean M-estimate (LMM) and NLMM. The method is evaluated on the MIT-BIH Polysomnographic Database
Tomasini et al. [19]	2016	ECG, EMG	A wearable platform is described for biopotential acquisition with no PLI noise. The hardware platform is evaluated using digital notch filters, subtraction approach, sinusoidal modeling approach and adaptive filters [20]. The performance of PLI removal in real time. The lowest computational cost is achieved by the adaptive filter which requires only 36 μs at each sample
b. Wavelet transform			
Gallianno Merino et al. [21]	2013	EMG	Proposes a method which isolates the 50-Hz fundamental component and its harmonics using a shift invariant transform. Then the PLI is reconstructed using the Discrete Stationary Wavelet Packet Transform (DSWPT). The method is evaluated on both synthetic and real EMG signals and then it outperforms traditional band stop filters and adaptive filters. In a recent review [10], this PLI cancelation scheme was applied for removing PLI from abdominal signals in order to extract the fECG. It obtained the best results in two testing scenarios (PLI with fixed 50-Hz fundamental frequency, and with harmonics,

Time-varying pole radius multiple notch filters			
Authors	**Year**	**Biopotentials**	**Observations**
			respectively). However, it is not working when the PLI has time varying fundamental frequency [10]
c. EMD			
Pal et al. [11]	2012	ECG	The PLI is extracted from ECG recordings based on the fact that high-frequency components are isolated in the first obtained Intrinsec Mode Functions (IMF). Cumulative mean and the power of the IMFs are used to decide which IMFs component contains PLI. However, when the PLI has similar power as the signal of interest, the robustness of the method decreases.
d. Hybrid methods			
Suchetha et al. [22]	2013	ECG	Proposes an adaptive filter and subtraction scheme both based on EMD. The performance is evaluated on synthetic ECG signals and various noise levels (from 5 to 30%). The direct subtraction method based on EMD shows the best results
Taralunga et al. [23]	2015	fECG	An adaptive filter based on HHT is proposed. The internal generated PLI reference is obtained using the Hilbert Transform to identify the IMFs, obtained with EMD, which contains the PLI and its harmonics. This internal generated PLI reference is further used in the LMS adaptive filter. The method is evaluated on fECG signals contaminated with different PLI levels. It is also considered the scenario when the fundamental frequency is not fixed. High performance is reported in all scenario considered, preserving the morphology of the fECG
Jenkal et al. [24]	2016	ECG	The algorithm consists of three steps: first the signal is the decomposition with the Discrete Wavelet Transform (DWT); next an adaptive dual threshold filter (ADTF) is applied and finally a peak correction is applied for the ECG signal in order to compensate for possible information loss during the PLI removal. The performance is evaluated on a real ECG signal, which is contaminated with synthetic PLI
Warmerdam et al. [25]	2016	ECG	A fixed-lag Kalman smoother with adaptive noise estimation is proposed. The performance of the algorithm is analyzed on simulated and real signals and compared with the performance obtained by a fixed-bandwidth notch filter and some adaptive filters. A better SNR and transient time are reported
Mateo et al. [26]	2015	ECG, EEG	The authors introduce a radial basis function Wiener hybrid filter for removing the PLI from ECG and EEG recordings. Real signal is used, recorded from 100 subjects (adults and children). The PLI signal was simulated with a 50 Hz sinusoidal with the fundamental frequency varying from 48.5 Hz to 51.5 Hz. The proposed method outperforms the classical Wiener filter

Table 1. Contributions in the field of PLI removing from biopotentials in the last 5 years.

in order to decompose the ECG signal into intrinsic mode functions (IMFs). Then the IMFs that contain the PLI signal are discarded, and the signal is reconstructed. However, the ECG information is not isolated in one IMF and its high-frequency components, that is, the QRS complex can be present in the discarded IMFs. An approach to recover some lost information consists of identifying the IMFs that contain QRS complexes and the QRS complexes boundaries. Next, a Tukey window centered on the R peaks is applied which offers a flat gain for the R wave. Thus, the information of the QRS complex is preserved.

http://dx.doi.org/10.5772/intechopen.74579

4. Case study: the influence of fixed-bandwidth notch filters on the diagnostic information in ECG signals

In this section, the most basic, simplest and common approaches for PLI and its harmonics removal from ECG recordings is evaluated. Mainly, the loss of diagnostic information in the process of PLI removal is analyzed. In order to achieve this objective, four types of traditional fixed frequency band stop filters and a time-varying pole radius multiple notch IIR filter [12] are implemented in MATLAB and tested on a real ECG database.

4.1. Diagnostic information in ECG signals

The ECG signal is generated by the electrical activity of the cardiac tissue. It reflects differences in transmembrane voltages in myocardial cells that occur during depolarization and repolarization within each cardiac cycle [26]. By placing a specific electrode configuration on the human body, a projection of this electrical activity on the measurement lead can be recorded. The electrode configuration can be both bipolar (the three bipolar Einthoven derivations) and unipolar (the three augmented derivations and the six precordial ones).

The ECG signal is depicted in **Figure 6** and mainly consists of five waves: P wave, Q wave, R wave, S wave and T wave and U wave. The P wave corresponds to the electrical depolarization of the atrial cardiac tissue. The ventricular contraction generates the QRS and the electrical repolarization of the ventricular tissue generates the T wave. The U wave most likely represents an electric-mechanical phenomenon that occurs after repolarization is completed [27]. In

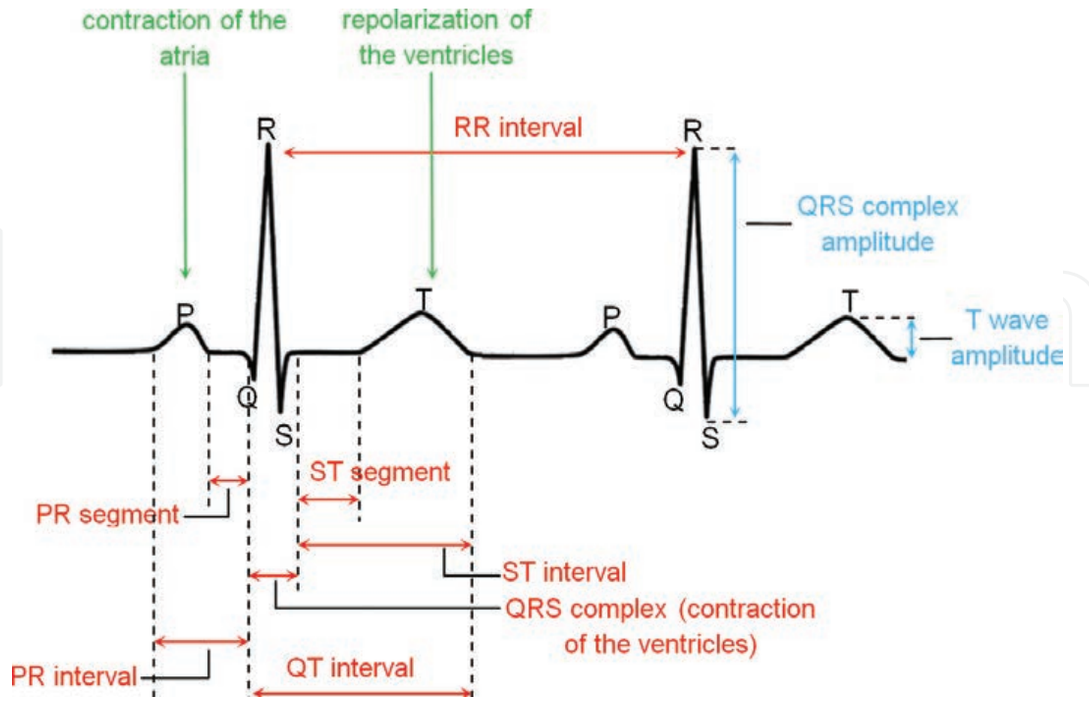

Figure 6. The waveforms, interval and segments of the ECG signal.

Figure 6, also the parameters of the ECG signal can be observed: the intervals (PR, QT, ST) and the segments (PR, ST).

The amplitude and the morphology of the ECG waves, segments and intervals represent the basic diagnostic information. Based on the analysis of these parameters, the health status of the heart can be investigated.

In **Table 2**, a small selection of abnormal electrical behavior of the heart and the influence of the ECG parameters is presented.

Thus, width, duration and amplitude measurements of the ECG waves are used to define abnormal electrical conduction in the heart, to detect cardiac tissue damage, and to classify patients at risk of cardiac arrhythmias.

4.2. Data used in the case study

The data used in this study are available from the Physionet QT interval database [28]. It contains a wide variety of QRS and ST-T morphologies and includes 105 ECG records taken from the following ECG databases: MIT-BIH Arrhythmia Database [29], the European Society of Cardiology ST-T Database [30], MIT-BIH Supraventricular Arrhythmia Database [27], The MIT-BIH Long-Term Database [31], MIT-BIH Normal Sinus Rhythm Database [32], Sudden Cardiac Death Holter Database [33] and MIT-BIH ST Change Database [34].

The data are sampled at 250 Hz and have annotations for the beginning and the end of P wave, QRS complex and T wave (**Figure 7**). For this study, 17 ECG recordings are used: sel51,

Some electrical abnormalities of the heart	ECG parameters characteristics
1. Sino-atrial (SA) block—type2	• PR segment is constant • For one, two, or three cycles, the P wave is missing (no firing of the SA node)
2. Atrio-ventricular (AV) block—1st degree	• PR segment is longer than normal, PR segment >300 ms • The P waves are superimposed on the T waves
3. AV block—2nd degree, Mobitz I	• The PR segments increases its length progressively culminating in an absence of QRS waves • The PR is the longest immediately before the dropped of the QRS waves • The PR is the shortest immediately after the dropped QRS waves
4. AV block—3rd degree (complete heart block)	• There is no relation between the frequency of the atrias contraction and the one of the ventricles contraction. Thus, the PR segment and interval have random lengths in each cardiac cycle
5. Atrial fibrillation	• Absence of P wave • Irregular RR interval • Random oscillations in the place of the P wave
6. Atrial flutter	
7. Intracranial hemorrhage	• Giant T-wave inversion [23]

Table 2. A few abnormal electrical behaviors of the heart and the influence on the ECG parameters.

http://dx.doi.org/10.5772/intechopen.74579

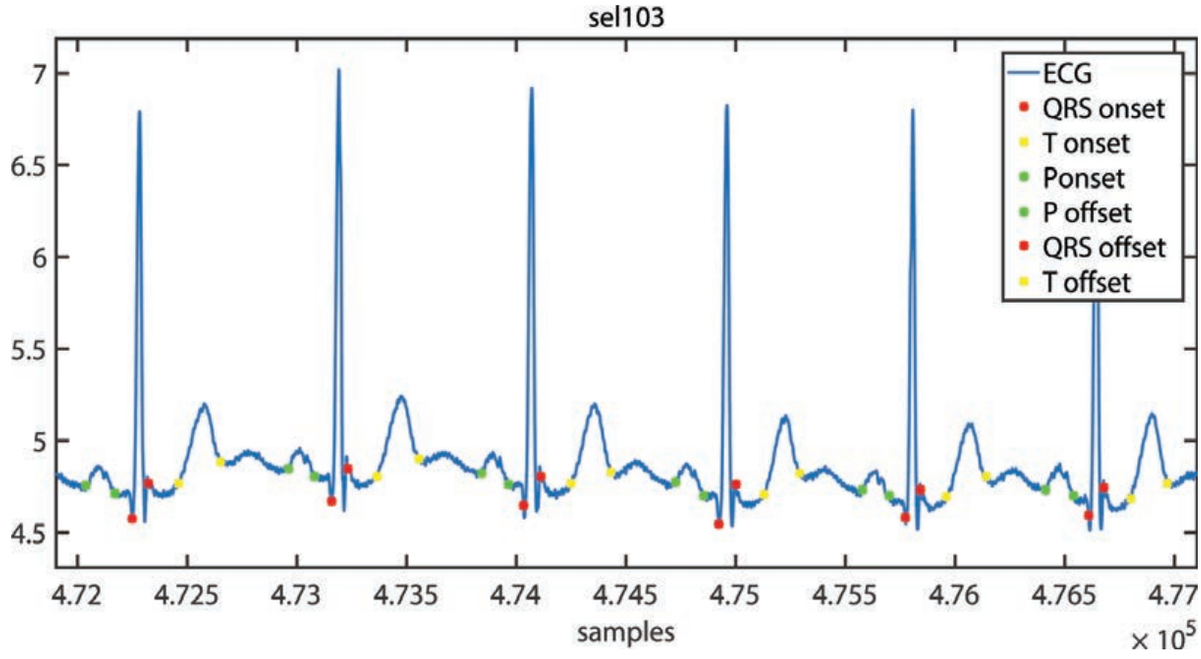

Figure 7. An ECG example with marked onset and offset for P, QRS and T waves.

sel103, sel302, sel306, sel307, sel808, sel872, sel16483, sel16786, sel17453, sele0121, sele0122, sele0170, sele0303, sele0509, sele0606, sele0607.

The real ECG signals are contaminated with synthetic PLI generated using 50 Hz and 150 Hz sine waves and having SNR = −2 dB:

$$PLI(t) = A_1 \cdot \sin\left(2\pi f_1 t\right) + A_3 \cdot \sin\left(2\pi f_3 \cdot t\right), f_1 = 50\ Hz,\ \ f_3 = 150\ Hz, A_3 = kA_1 \tag{1}$$

4.3. Digital filters

Four types of traditional IIR band stops filters are considered: Butterworth, Chebyshev I, Chebyshev II and elliptic. Cascaded filters from each type are implemented with the following stop bands: 49.5–50.5 Hz and 149.5–150.5 Hz. Their performance is compared against the time-varying pole radius multiple notch IIR filter [12] defined by the following equations:

$$H(z) = \prod_{i=1}^{K} \frac{1 - 2\cos\left(\Omega_{\mathrm{Ni}}\right)\mathrm{z}^{-1} + \mathrm{z}^{-2}}{1 - 2rcos(\Omega_{\mathrm{Ni}})\mathrm{z}^{-1} + \mathrm{r}^2\mathrm{z}^{-2}} = \frac{B(z)}{B(r^{-1}z)},\ \ B(z) = \sum_{i=0}^{2K} b_i \mathrm{z}^{-\mathrm{i}} \tag{2}$$

where K is the number of notches, Ω_{Ni} is the central frequency of the notch, N is the order of the harmonics, $B(z)$ is a symmetrical polynomial and r is the pole radius. In (3), the difference equation of the IIR multiple notch filter with a time-varying parameter r is presented:

$$\begin{aligned} y(n) = {} & b_0 x(n) + b_1 x(n-1) + \cdots + b_{2K} x(n-2K) \\ & - r(n) b_1 y(n-1) - \cdots - r^{2K}(n) b_{2K} y(n-2K) \end{aligned} \tag{3}$$

where the variation of $r(n)$ is:

$$r(n) = \overline{r}\left(1 + (d_r - 1)e^{-\frac{n}{vf_s}}\right), n \geq 0, \tag{4}$$

with variation range $d_r = r(0)/\overline{r}$ and $\overline{r} = \lim_{n\to\infty} r(n)$; v includes the exponential variation of $r(n)$ in (3), and f_s is the sampling frequency [7].

4.4. Performance measurements

The performance analysis is focused on the ST segment. Thus, 19,715 ST segments are included in the case study from the 20 ECG recordings. Three performance indices are considered:

- Mean square error (MSE):

$$MSE_j = \frac{1}{N}\sum_{i=1}^{N}\left(ST_{orig\_j}(i) - ST_{est\_j}(i)\right)^2 \tag{5}$$

  where N is the number of samples of a ST segment, $j = \overline{1 \ldots M}$, M is the total number of ST segments ($M = 19,715$), ST_{orig} is the ST segment from the clean ECG recording, before PLI contamination and ST_{est} is the ST segment obtained after the filters are applied for PLI and its harmonic cancelation;

- Normalized root mean square error (NRMSE):

$$NRMSE_j = \sqrt{\frac{\sum_{i=1}^{N}\left(ST_{orig\_j}(i) - ST_{est\_j}(i)\right)^2}{\sum_{i=1}^{N}\left(ST_{orig\_j}(i) - \overline{ST_{orig\_j}}\right)^2}} \tag{6}$$

- Noise retention expressed in percentage

$$NR_j = \frac{P_{STorig\_j} - P_{STest\_j}}{P_{STorig\_j}} \times 100 \tag{7}$$

  where $P_{STorig} = 10\log_{10}\sum_{i=1}^{N}\left(ST_{orig}(i)\right)^2$

4.5. Results

In **Figure 8**, a segment from the ECG sel103 record is displayed before and after the contamination with synthetic PLI.

Figure 9 depicts a detail from the ECG sel16773 after the digital filters are applied for PLI and its harmonic cancelation, and in **Figure 10**, a zoom of the ST segment from the ECG cycle presented in **Figure 9** is displayed.

http://dx.doi.org/10.5772/intechopen.74579

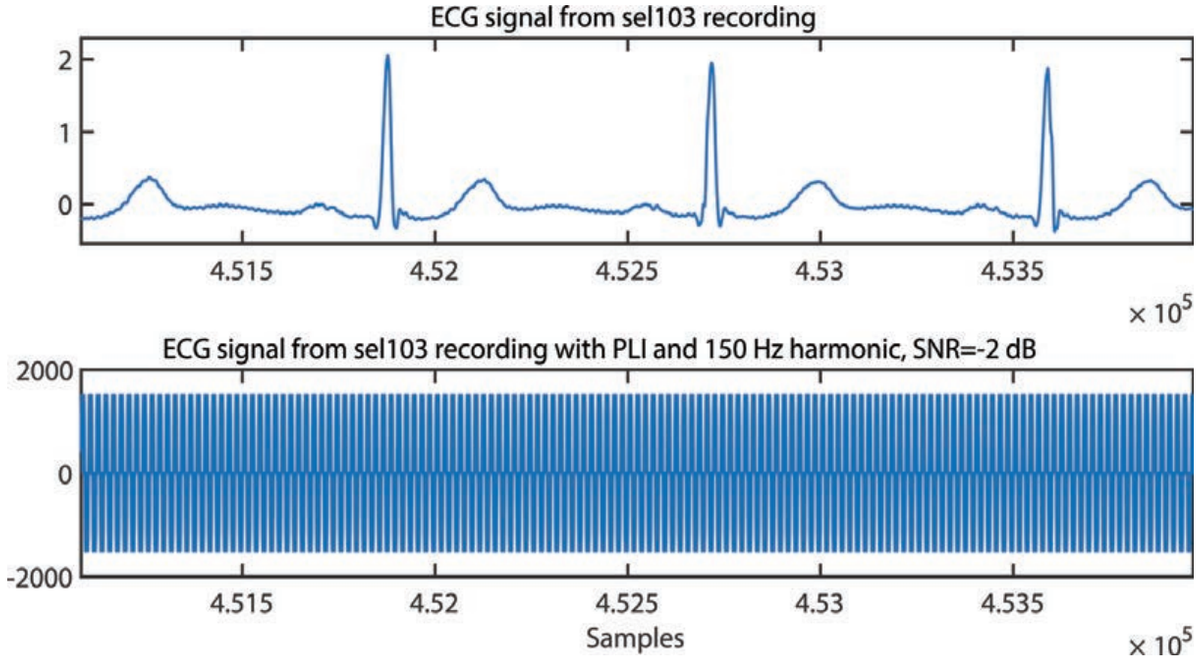

Figure 8. Upper subplot: clean ECG signal; lower subplot: ECG signal with PLI and its harmonics (SNR = −2 dB).

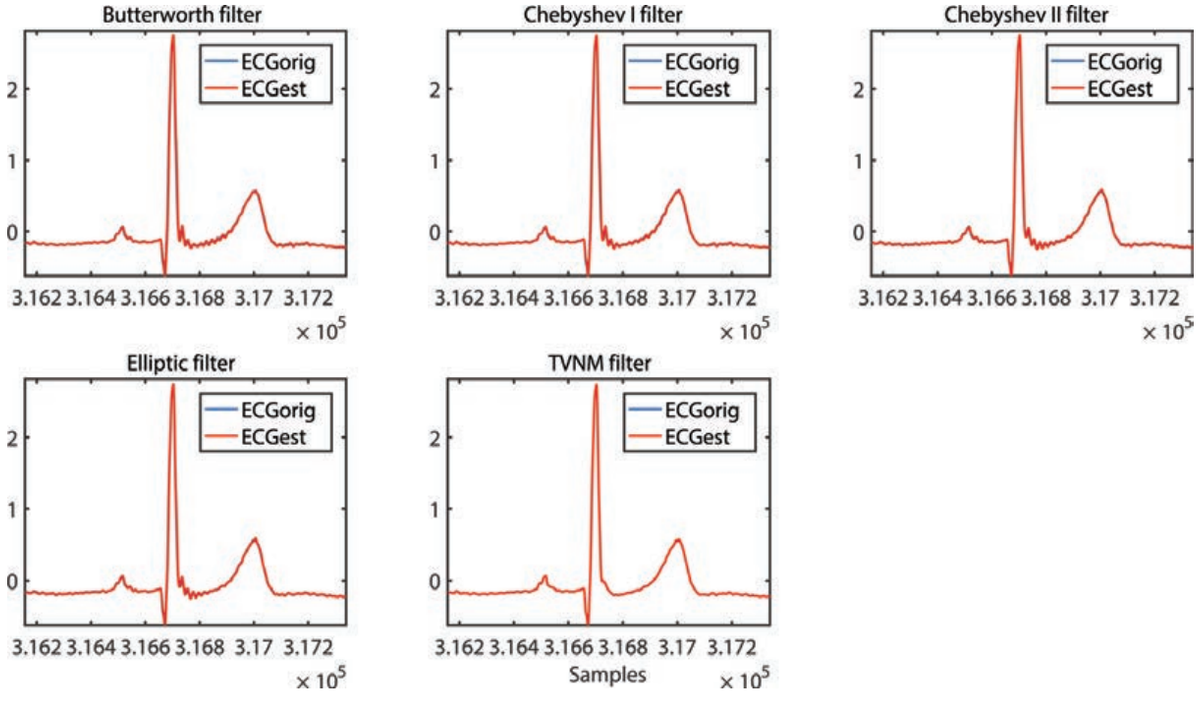

Figure 9. ECG sel16773 after the digital filters is applied. The estimated ECG signal is depicted with red.

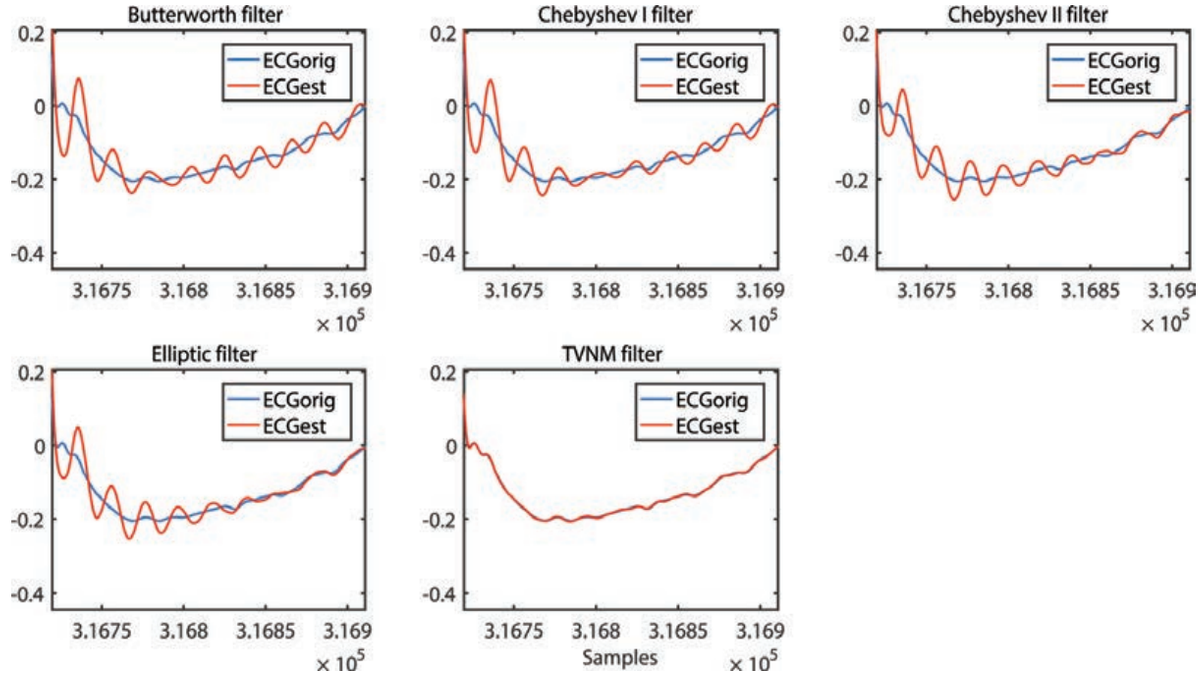

Figure 10. Detail on a ST segment. The estimated ECG signal is depicted with red.

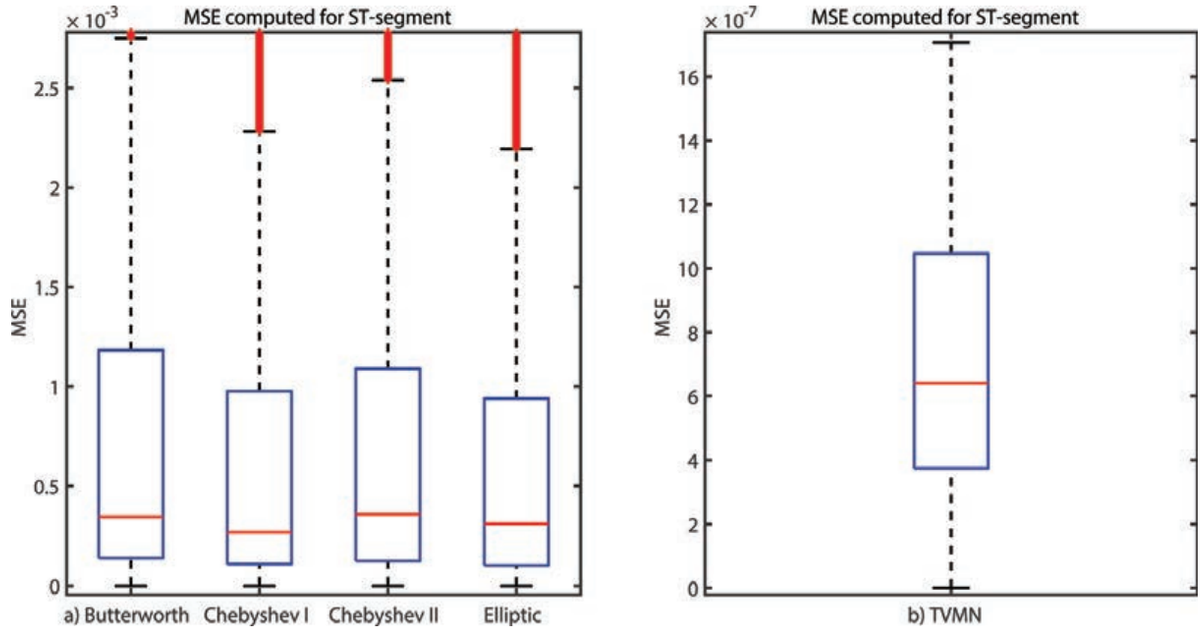

Figure 11. MSE determined for all 19,715 ST segments: (a) after the digital traditional band stop filters are applied; (b) after the TVMN is applied.

Figures 11–13 illustrate boxplots for the MSE, NRMSE and NR respectively, across all 19,715 ST segments. The results for TVNM are depicted in separated subplots because the indices computed in this case have very different values (much smaller).

http://dx.doi.org/10.5772/intechopen.74579

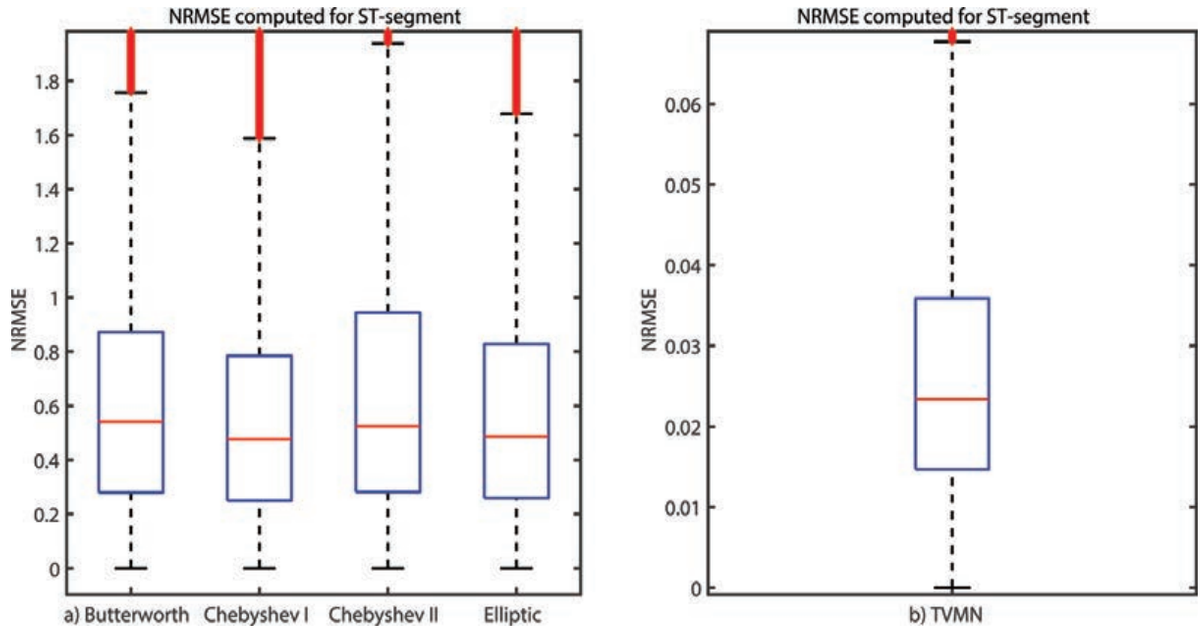

Figure 12. NRMSE determined for all 19,715 ST segments: (a) after the digital traditional band stop filters are applied; (b) after the TVMN is applied.

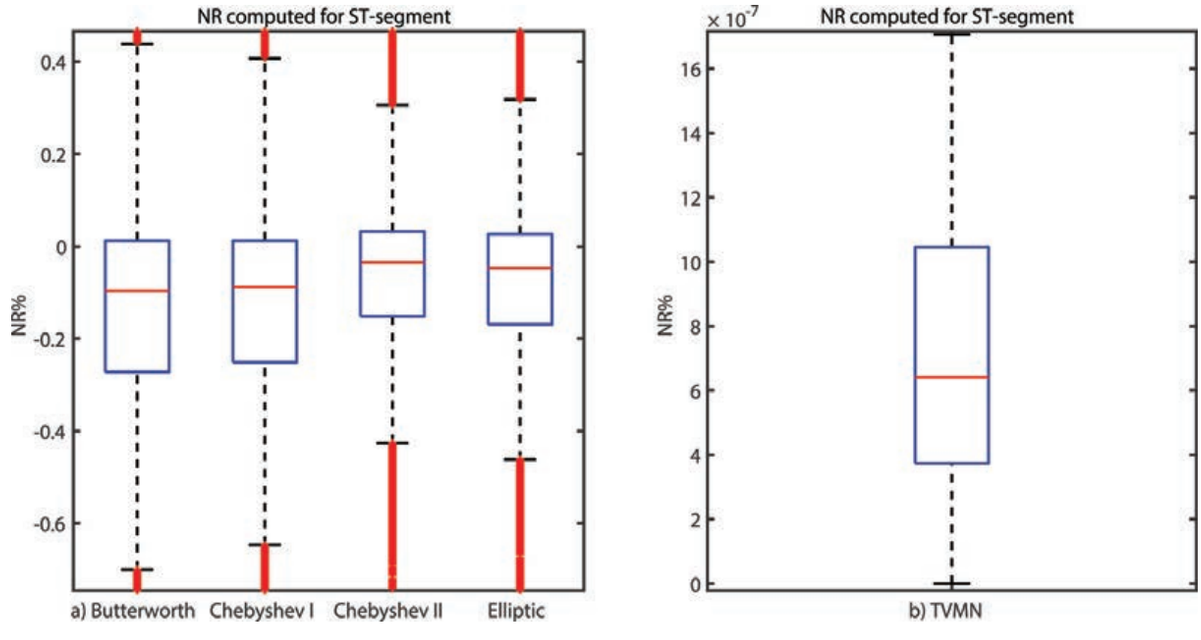

Figure 13. NR determined for all 19,715 ST segments: (a) after the digital traditional band stop filters are applied; (b) after the TVMN is applied.

4.6. Conclusions

The digital traditional band stop filters introduce a ringing effect, especially after the QRS complex, which show the highest ECG frequency components. This can be observed in **Figures 9** and **10**. Also, the performance indices computed for 19,715 ST segments confirm

the presence of the distortion introduced by the filters. All four traditional filters have similar performance. In contrast, the TVNM filter has far better performance with indices having the values 10–100 times smaller. TVNM introduces almost no distortion (**Figures 9** and **10**). The ringing effect introduced by the traditional filters can impair the ST segment identification, and so the physician diagnostic. Moreover, the impact is not only when discussing the health status of the adult heart but also when considering the fetal heart diagnosis. fECG is an important clinical tool to evaluate the wellbeing of the fetus during pregnancy. In particular, the ST segment from the fECG has strong diagnostic power. Changes in fetal ST segment can indicate fetal hypoxia, myocardial dystrophy, cardiac malformations, and so on. Thus, the residuals of the traditional filters will have a greater impact on the fECG parameters because this signal has much smaller power than the adult ECG. Hence, traditional band stop filters should be avoided if the parameters of the ECG are to be extracted.

On the other hand, the TVNM shows no ringing effect and the resulted ECG signal after the PLI and its harmonic removal is almost identical with the original ECG. Hence, the risk of misreading the ECG parameters is almost nonexistent. In addition, in comparison with the traditional filters, it has a very short transient time.

Author details

Țarălungă Dragoș Daniel* and Mihaela Neagu (Ungureanu)

*Address all correspondence to: dragos.taralunga@upb.ro

Department of Applied Electronics and Information Engineering, Politehnica University, Faculty of Electronics, Telecommunications and Information Technology, Bucharest, Romania

References

[1] IEEE Recommended Practice and Requirements for Harmonic Control in Electric Power Systems. IEEE Std 519-2014 (Revision of IEEE Std 519-1992). 2014;1-29. DOI: 10.1109/IEEESTD.2014.6826459

[2] Umeh KC, Mohamed A, Mohamed R. Comparing the harmonic characteristics of typical single-phase nonlinear loads. In: Proceedings. National Power Engineering Conference; 2003. pp. 383-387. DOI: 10.1109/PECON.2003.1437479

[3] Saraiva F d O, Bernardes WMS, Asada EN. A framework for classification of non-linear loads in smart grids using artificial neural networks and multi-agent systems. Neurocomputing. 2015;**170**:328-338. DOI: 10.1016/j.neucom.2015.02.090

[4] Arthur R, Shanahan RA. Neutral currents in three phase wye systems. Power Systems Engineering Data. 1996:0104ED9501R8/96

[5] Widrow B, Glover JR Jr, McCool JM. Adaptive noise cancelling: Principles and applications. Proceedings of the IEEE. 1975;**63**(12):1692-1716

[6] Li H, Zhang J, Wang L. A fully integrated continuous-time 50-Hz notch filter with center frequency tunability. In: Annual International Conference of the IEEE Engineering in Medicine and Biology Society; Boston. 2011. pp. 3558-3562. DOI: 10.1109/IEMBS.2011.6090593

[7] Huhta JC, Webster JG. 60-Hz interference in electrocardiography. IEEE Transactions on Biomedical Engineering. 1973;BME-**20**(2). DOI: 10.1109/TBME.1973.324169

[8] Guermandi M, Scarselli EF, Guerrieri R. A driving right leg circuit (DgRL) for improved common mode rejection in bio-potential acquisition systems. IEEE Transactions on Biomedical Circuits and Systems. 2016;**10**(2):507-517. DOI: 10.1109/TBCAS.2015.2446753

[9] Gomez-Clapers J, Serrano-Finetti E, Casanella R Pallas-Areny R. Can driven-right-leg circuits increase interference in ECG amplifiers. In: Annual International Conference of the IEEE Engineering in Medicine and Biology Society; Boston. 2011. pp. 4780-4783. DOI: 10.1109/IEMBS.2011.6091184

[10] Ţarălungă D-D, Ungureanu G-M, Gussi I, Strungaru R, Wolf W. Fetal ECG extraction from abdominal signals: A review on suppression of fundamental power line interference component and its harmonics. Computational and Mathematical Methods in Medicine. 2014;**2014**:Article ID 239060. DOI: 10.1155/2014/239060

[11] Pal S, Mitra M. Empirical mode decomposition based ECG enhancement and QRS detection. Computers in Biology and Medicine. 2012;**42**(1):83-92. DOI: 10.1016/j.compbiomed.2011.10.012

[12] Piskorowski J. Suppressing harmonic powerline interference using multiple-notch filtering methods with improved transient behavior. Measurement. 2012;**45**(6):1350-1361. DOI: 10.1016/j.measurement.2012.03.004

[13] Piskorowski J. Time-efficient removal of power-line noise from EMG signals using IIR notch filters with non-zero initial conditions. Biocybernetics and Biomedical Engineering. 2013;**33**(3):171-178. DOI: 10.1016/j.bbe.2013.07.006

[14] Pei S-C, Tseng C-C. Elimination of AC interference in electrocardiogram using IIR notch filter with transient suppression. IEEE Transactions on Biomedical Engineering. 1995; **42**(11):1128-1132. DOI: 10.1109/10.469385

[15] Rana KPS, Kumar V, Gupta A. A pole-radius-varying IIR notch filter with enhanced post-transient performance. Biomedical Signal Processing and Control. 2017;**33**:379-391. DOI: 10.1016/j.bspc.2016.12.015

[16] Wang Q, Gu X, Lin J. Adaptive notch filter design under multiple identical bandwidths. AEU—International Journal of Electronics and Communications. 2017;**82**:202-210. DOI: 10.1016/j.aeue.2017.08.054

[17] Razzaq N, Sheikh SAA, Salman M, Zaidi T. An intelligent adaptive filter for elimination of power line interference from high resolution electrocardiogram. IEEE Access. 2016;**4**: 1676-1688

[18] Lin J, Sun X, Wu J, Chan SC, Xu W. Removal of power line interference in EEG signals with spike noise based on robust adaptive filter. In: IEEE Region 10 Conference, TENCON; Singapore. 2016. p. 2707-2710

[19] Tomasini M, Benatti S, Milosevic B, Farella E, Benini L. Power line interference removal for high-quality continuous biosignal monitoring with low-power wearable devices. IEEE Sensors Journal. 2016;**16**(10):3887-3895

[20] Keshtkaran MR, Yang Z. A robust adaptive power line interference canceler VLSI architecture and ASIC for multichannel biopotential recording applications. IEEE Transactions on Circuits and Systems II: Express Briefs. 2014;**61**(10):788-792. DOI: 10.1109/TCSII.2014.2345302

[21] Galiana-Merino JJ, Ruiz-Fernandez D, Martinez-Espla JJ. Power line interference filtering on surface electromyography based on the stationary wavelet packet transform. Computer Methods and Programs in Biomedicine. 2013;**111**(2):338-346

[22] Suchetha M, Kumaravel N. Empirical mode decomposition based filtering techniques for power line interference reduction in electrocardiogram using various adaptive structures and subtraction methods. Biomedical Signal Processing and Control. 2013;**8**(6):575-585. DOI: 10.1016/j.bspc.2013.05.001

[23] Taralunga DD, Gussi I, Strungaru R. Fetal ECG enhancement: Adaptive power line interference cancellation based on Hilbert Huang transform. Biomedical Signal Processing and Control. 2015;**19**:77-84. DOI: 10.1016/j.bspc.2015.03.009

[24] Jenkal W, Latif R, AhmedToumanari AD, El B'charri O, Maoulainine FMR. An efficient algorithm of ECG signal denoising using the adaptive dual threshold filter and the discrete wavelet transform. Biocybernetics and Biomedical Engineering. 2016;**36**(3):499-508. DOI: 10.1016/j.bbe.2016.04.001

[25] Warmerdam GJJ, Vullings R, Schmitt L, Van Laar JOEH, Bergmans JWM. A fixed-lag Kalman smoother to filter power line interference in electrocardiogram recordings. IEEE Transactions on Biomedical Engineering. 2017;**64**(8):1852-1861. DOI: 10.1109/TBME.2016.2626519

[26] Mateo J, Sánchez-Morla EM, Santosd JL. A new method for removal of powerline interference in ECG and EEG recordings. Computers & Electrical Engineering. 2015;**45**:235-248. DOI: 10.1016/j.compeleceng.2014.12.006

[27] Kligfield P, Gettes LS, Bailey JJ, Childers R, Deal BJ, William Hancock E, van Herpen G, Kors JA, Macfarlane P, Mirvis DM, Pahlm O, Rautaharju P, Wagner GS. Recommendations for the standardization and interpretation of the electrocardiogram. Circulation. 2007;**115**:1306-1324. DOI: 10.1161/CIRCULATIONAHA.106.180200

[28] Rautaharju PM, Surawicz B, Gettes LS. AHA/ACCF/HRS recommendations for the standardization and interpretation of the electrocardiogram. Part IV: The ST segment, T and U waves, and the QT interval. Circulation. 2009;**119**:e241-e250

[29] Goldberger AL, Amaral LAN, Glass L, Hausdorff JM, Ivanov PC, Mark RG, Mietus JE, Moody GB, Peng C-K, Stanley HE. PhysioBank, PhysioToolkit, and PhysioNet: Components

of a new research resource for complex physiologic signals. Circulation. 2000;**101**(23): e215-e220

[30] Moody GB, Mark RG. The MIT-BIH Arrhythmia Database on CD-ROM and software for use with it. In: Proceedings Computers in Cardiology; Chicago, IL. 1990. pp. 185-188. DOI: 10.1109/CIC.1990.144205

[31] Taddei A, Biagini A, et al. The European ST-T database: Development, distribution and use. In: Proceedings Computers in Cardiology; Chicago, IL. 1990. pp. 177-180

[32] Greenwald SD, Patil RS, Mark RG. Improved detection and classification of arrhythmias in noise-corrupted electrocardiograms using contextual information. In: Proceedings Computers in Cardiology; Chicago, IL. 1990. pp. 461-464. DOI: 10.1109/CIC.1990.144257

[33] Greenwald SD. The development and analysis of a ventricular fibrillation detector [dissertation]. Massachusetts Institute of Technology. Department of Electrical Engineering and Computer Science: Massachusetts Institute of Technology; 1986. Available from: http://hdl.handle.net/1721.1/92988

[34] Albrecht P. ST segment characterization for long term automated ECG analysis [dissertation]. Massachusetts Institute of Technology, Department of Electrical Engineering and Computer Science: Massachusetts Institute of Technology; 1983. 378 p